RESEARCH ARTICLE

Global Change Biology WILEY

How drought events during the last century have impacted biomass carbon in Amazonian rainforests

Yitong Yao[1] | Philippe Ciais[1] | Nicolas Viovy[1] | Emilie Joetzjer[2] | Jerome Chave[3]

[1]Laboratoire des Sciences du Climat et de l'Environnement, LSCE/IPSL, CEA-CNRS-UVSQ, Université Paris-Saclay, Gif-sur-Yvette, France

[2]INRAE, Universite de Lorraine, AgroParisTech, UMR Silva, Nancy, France

[3]Laboratoire Evolution et Diversité Biologique UMR 5174 CNRS, IRD, Université Paul Sabatier, Toulouse, France

Correspondence
Yitong Yao, Laboratoire des Sciences du Climat et de l'Environnement, LSCE/IPSL, CEA-CNRS-UVSQ, Université Paris-Saclay, Gif-sur-Yvette 91191, France.
Email: yitong.yao@lsce.ipsl.fr

Abstract

During the last two decades, inventory data show that droughts have reduced biomass carbon sink of the Amazon forest by causing mortality to exceed growth. However, process-based models have struggled to include drought-induced responses of growth and mortality and have not been evaluated against plot data. A process-based model, ORCHIDEE-CAN-NHA, including forest demography with tree cohorts, plant hydraulic architecture and drought-induced tree mortality, was applied over Amazonia rainforests forced by gridded climate fields and rising CO_2 from 1901 to 2019. The model reproduced the decelerating signal of net carbon sink and drought sensitivity of aboveground biomass (AGB) growth and mortality observed at forest plots across selected Amazon intact forests for 2005 and 2010. We predicted a larger mortality rate and a more negative sensitivity of the net carbon sink during the 2015/16 El Niño compared with the former droughts. 2015/16 was indeed the most severe drought since 1901 regarding both AGB loss and area experiencing a severe carbon loss. We found that even if climate change did increase mortality, elevated CO_2 contributed to balance the biomass mortality, since CO_2-induced stomatal closure reduces transpiration, thus, offsets increased transpiration from CO_2-induced higher foliage area.

KEYWORDS
Amazon rainforest, drought sensitivity, net forest carbon sink, process-based model, tree mortality

1 | INTRODUCTION

The Amazonian rainforest accounts for 40% of the tropical forest biome area and contains half of its carbon. Changes in the Amazon forest dynamics impact the global water and carbon cycles and exert key feedback on climate change (Jimenez & Takahashi, 2019), leaving open the possibility of crossing 'tipping points' in the form of regional forest dieback (Ritchie et al., 2021). Both short-term variability and long-term trends in the carbon fluxes and stocks of the

forest are regulated by climate variability. In particular, repeated extreme drought events have the potential to undermine the stability of large parts of the Amazon forest (Zemp et al., 2017). Over the last century, major drought events occurred in Amazonia, generally associated with positive sea surface temperature anomalies in the tropical Atlantic (1916, 1963, 2005, 2010) and with strong El Niño events (1926, 1982/83, 1997/98, 2015/16). El Niño events tend to bring drought in the wet season, whereas Atlantic anomalies exacerbate drought in the dry season (Jimenez et al., 2018).

While the long-term view is crucial to understand the current dynamics of Amazonia, much of our knowledge about the response of Amazonian forests to drought is based on limited field data from the last decades: a slow-down of forest carbon gains from growth and a coincident increase of losses from tree mortality have been observed from successive forest plot inventories, leading to a gradual decline in the strength of the biomass carbon sink (Brienen et al., 2015).

Research focusing on past drought events used different methods, including ground-based observations of carbon fluxes at few sites (Doughty et al., 2015), biomass inventories (Feldpausch et al., 2016; Phillips et al., 2009), drought experiments (Fisher et al., 2007), remote-sensing (Yang et al., 2018), and process-based models (Papastefanou et al., 2021). Analyses from the RAINFOR network of forest plots provided net biomass change at selected locations during the 2005 and 2010 droughts (Feldpausch et al., 2016; Hubau et al., 2020), and spatial patterns in variation of mortality rates (Esquivel-Muelbert et al., 2020) and biomass loss (Papastefanou et al., 2022).

Ground-based observations and satellite products only cover climatic anomalies for two decades, a short timescale compared with the natural dynamics of forests. A centennial perspective is needed, as repeated droughts affect decadal-scale carbon processes through legacy effects and slow recovery of forests after disturbances (Lewis et al., 2011). Given the lack of observations, process-based models are useful to explore the effects of drought on the Amazon carbon balance.

Although predicting the risk of mortality from hydraulic failure is challenging given species-specific responses (Rowland et al., 2021), several process-based models have made progress in representing a mechanistic hydraulic architecture simulating the water transport through trees, from the soil to the atmosphere (Kennedy et al., 2019; Li et al., 2021). Leaf-level carbon-water trade-offs, reflecting plant stomatal strategies, are at the foundation of most hydraulic modules, and they are used in models as a target to be optimized, for example, the product of productivity and water cost (Eller et al., 2020) or the direct and opportunity carbon cost of xylem damage (Lu et al., 2020). Although these studies partly captured changes of plant hydrodynamics, they did not consider the water capacitance of trees (Kennedy et al., 2019) or did not model changes in the vertical profile of water potential from soil to leaves, rather focusing on stomatal behavior (Eller et al., 2020). A hydraulic architecture model describing explicit water transport process is required to better mimic plant water dynamics in reality. Yao et al. (2022) simulated half-hourly water potentials at leaf, stem, root and soil levels by minimizing the difference between water demand and supply for each plant organ in the ORCHIDEE-CAN-NHA model, a branch of the ORCHIDEE land surface model (version r7236). In addition to representing changes in water flows and storage on a 30 min time-step in soils and plants, this model includes an empirical parameterization of mortality from hydraulic failure. Namely, when

stem water conductance drops below a critical threshold during a certain number of days, a mortality risk function is calculated and trees of each cohort die if this function exceeds a threshold. The advantage of ORCHIDEE-CAN lies in its explicit representation of different tree-size cohorts, which allows us to link realization of simulation of hydrodynamics to forest demography. The model was calibrated against field observations from the Caxiuanã throughfall exclusion (TFE) experiment (Fisher et al., 2007) and tested on another TFE experiment site at Tapajos. Yet, it has not been used to assess the carbon impacts of regional drought. Here, we address this challenge by applying this model over rainforest in the Amazon basin during the last century.

Besides climate change, an important consideration for modelling the carbon balance of the Amazon over a century is that CO_2 concentration has increased by more than 120 ppm during this period. There is consensus on the stimulation effects on growth under elevated CO_2, although no field CO_2 enrichment experiment (FACE) is available for Amazonia. A simulated elevated CO_2 forcing predicted an increase in aboveground biomass for an ensemble of models but limited by phosphorus availability (Fleischer et al., 2019). Increased CO_2 concentration also affects carbon allocation, and self-thinning (Holm et al., 2020), and reduces stomatal conductance, resulting in less transpiration per unit of leaf area, although increased leaf area may act to counteract this effect (Cox et al., 2004; Piao et al., 2007). Yet, the effect of elevated CO_2 on stand competition and biomass loss processes is uncertain, especially with a higher drought frequency. Site-level spatial statistical analysis with CO_2 concentration and climatic factors by Hubau et al. (2020) suggested significant positive relationships of carbon gains with CO_2 concentration, but not of carbon loss. Process-based models can, thus, be used to tests to separate the effects of climate change and CO_2, and their interactions. de Almeida Castanho et al. (2016) conducted simulations to reproduce the individual and combined effects of climate change and elevated CO_2, but their model included a simple mortality module and was unable to capture the biomass loss from climate extremes.

In this study, we use a new process-based model with a detailed mechanistic hydraulic architecture and mortality arising from hydraulic failure, ORCHIDEE-CAN-NHA (r7236), to understand the sensitivity of biomass growth and mortality to drought events of the last century in the Amazon, and *to elucidate* the contribution of climate change and elevated CO_2. Our objectives are as follows: (1) to test the performance of the model for simulating the long-term trend of net carbon sink and its component gains and losses, (2) to compare simulated patterns of drought-induced changes of growth and mortality against forest plots observations, (3) to compare aboveground biomass (AGB) losses between different drought events, (4) to assess if the recent extreme drought events of the last 20 years had higher impacts on AGB than during previous droughts of the early part of the century; (5) to understand the interactions between rising CO_2 and droughts on AGB dynamics.

2 | MATERIALS AND METHODS

2.1 | The land surface model ORCHIDEE-CAN-NHA

In this study, we use the ORCHIDEE-CAN-NHA (r7236) land surface model, incorporating allometric-based carbon allocation, trees cohorts making the canopy structure with different growth of an average tree in each cohort and background mortality induced by self-thinning processes (Naudts et al., 2015) as well as a new mechanistic hydraulic architecture (Yao et al., 2022). The hydraulic module includes the dynamic root water uptake scheme proposed by Joetzjer et al. (2022) and a plant hydraulic model simulating water transport from water potentials gradient between soils and atmosphere, and water capacitance in roots, stems, and leaves. Besides this hydraulic architecture, a cavitation-induced mortality model was added. Two parameters are used to translate the percentage loss of stem conductance (PLC) simulated by the hydraulic module to mortality. A cumulated drought exposure index when PLC stays above a critical threshold defines a mortality risk. Under this risk, a fraction of trees is killed each day in the different cohorts of tree size. The new hydraulic architecture and mortality schemes were calibrated against the world's longest running drought experiments at Caxiuanã (Rowland et al., 2015), with overall good performances.

2.2 | Simulation framework

2.2.1 | Climate forcing

The gridded climate forcing used as input to ORCHIDEE-CAN-NHA is the CRUJRA v2.1 dataset (Harris, 2020; Harris et al., 2014; 2020; Kobayashi et al., 2015). CRUJRA v2.1 was constructed by re-gridding data from the Japanese Reanalysis Data (JRA) produced by the Japanese Meteorological Agency (JMA) adjusted to match the monthly observation-based Climatic Research Unit (CRU) TS 4.04 data (Harris et al., 2020). It provides 6-hourly meteorological variables from January 1901 to December 2019 at 0.5×0.5° spatial resolution.

2.2.2 | Simulation protocol

To balance the spatial resolution of our regional simulations with computing resources, the simulations were carried out at 1×1° horizontal spatial resolution over 1901–2019 (study region see Figure 1). We used a two-step spin-up to bring carbon and water pools in steady-state equilibrium. In the first step, the model is forced by re-cycling the climate forcing during 1901–1920 with a constant CO_2 concentration of 296ppm and no climate-induced mortality activated. Then after the end of the first spin-up, we re-ran the model still recycling the climate forcing of 1901–1920 but activating the mortality scheme. At the end of the second stage of spin-up, the
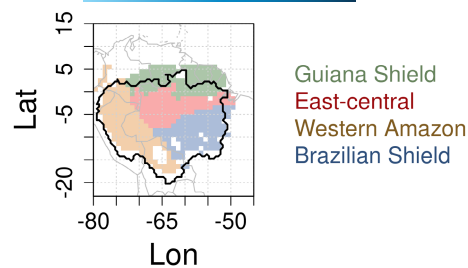

FIGURE 1 Overview of the Amazon basin, which is split into four regions, Guiana Shield, East-Central Amazon, Western Amazon, and Brazilian Shield, shown by different colors, defined after Feldpausch et al. (2011). The black line is the border of the Amazon basin from Papastefanou et al. (2022). Only pixels with tree cover more than 80% are shown. Map lines delineate study areas and do not necessarily depict accepted national boundaries.

model reaches a new equilibrium state, with a lower biomass due to droughts that occur periodically during 1901–1920, with less than 1% variation by the end of second spin-up. This equilibrium state serves as the starting point for three transient simulations during the historical period. To test the impact of the different drivers of CO_2, and climate we designed a series of factorial experiment S1, S2, S3, as described in Table 1.

2.3 | Drought characteristics

The maximum climatological water deficit (MCWD) is the most negative value of the difference between monthly precipitation and a fixed value for evapotranspiration of ~100mm among all the months (Equations 1 and 2). MCWD anomaly is derived after subtracting the mean MCWD over a baseline period. By locating the month with the most negative precipitation anomaly and its corresponding rainfall climatology interval, we distinguish between wet-season and dry-season drought by using a new drought timing index (DTI). A second index for the rain seasonality is defined as the deviation of monthly rainfall distribution from a uniform monthly distribution (Feng et al., 2013). Detailed description of these indices can be found in SI Notes S1.

$$CWD_m = CWD_{m-1} + P_m - 100 \text{ if } P_m < 100, \text{ else } CWD_m = 0 \tag{1}$$
$$\text{with m being the month1, } \ldots 12 \, (1 = October)$$

$$MCWD = \min(CWD_m), m = 1, \ldots, 12 \tag{2}$$

2.4 | How aboveground biomass dynamics was analyzed

From model outputs, net AGB change (ΔAGB), AGB gain and loss are calculated over the hydrological year from October in previous year to September in the next year. AGB gain is the carbon allocated to growth in aboveground sapwood in cohorts with DBH higher than 10 cm, each year. AGB loss is the biomass mortality of aboveground

TABLE 1 Description of simulations performed in this study

	Climate forcing	Atmospheric CO_2	Mortality module	Restart point
Spin-up stage 1	1901–1920	Constant (296 ppm)	Deactivate	/
Spin-up stage 2	1901–1920	Constant (296 ppm)	Activate	Stage1
S1	1901–1920	Increasing	Activate	Stage2
S2	1901–2019	Increasing	Activate	Stage2
S3	1901–2019	Constant (296 ppm)	Activate	Stage2

Note: In the S1 scenario, the model is forced by recycling the climate forcing data between 1901 and 1920 and the CO_2 concentration increases following the reality. In the S2 scenario, both climate forcing and CO_2 concentration vary. In the S3 scenario, the CO_2 concentration input to model is set constant as 296 ppm but climate forcing data varies.

sapwood and heartwood in cohorts with DBH higher than 10 cm, each year. ΔAGB is the difference between AGB gain and AGB loss. The anomaly during a drought year k is derived by subtracting the average value (μ) over a multi-year baseline period by Equations (3) to (5).

$$\Delta AGB_{anomaly} = \Delta AGB_k - \mu_{\Delta AGB} \tag{3}$$

$$AGBgain_{anomaly} = AGBgain_k - \mu_{AGBgain} \tag{4}$$

$$AGBloss_{anomaly} = AGBloss_k - \mu_{AGBloss} \tag{5}$$

Biomass mortality from self-thinning and droughts are included. In our study, the mortality rate equals the number of dead trees per year divided by the number of trees alive in the beginning of 1 year.

3 | RESULTS

3.1 | Long-term trend of the biomass carbon sink, model versus inventories

In our simulation S2 with variable CO_2 and climate, we found a mean positive value of ΔAGB equal to 0.22 MgC ha^{-1} year^{-1} over 1980–2019, indicating that the Amazon intact forests accumulate carbon over time. Nevertheless, this increase of ΔAGB has a negative trend of 0.006 Mg C ha^{-1} year^{-2} (Figure 2). This slowing down of the biomass carbon sink occurs because carbon losses from mortality increase faster than gains from growth and recruitment. Our finding of a decreasing biomass sink is consistent with inventory data analyzed by Hubau et al. (2020) and Brienen et al. (2015). Yet the magnitudes of the simulated growth trend and loss trend are both smaller than in the observations. We simulated an increasing trend of carbon gains of 0.008 Mg C ha^{-1} year^{-2} against 0.014 Mg C ha^{-1} year^{-2} for carbon losses across the entire basin. In comparison, Hubau et al. (2020) from 321 plots found an increasing trend of gain of 0.014 Mg C ha^{-1} yr^{-2} and a trend of loss of 0.023 Mg C ha^{-1} year^{-2}. This difference can be attributed to limited coverage of inventory sample plots and model limitations, such as
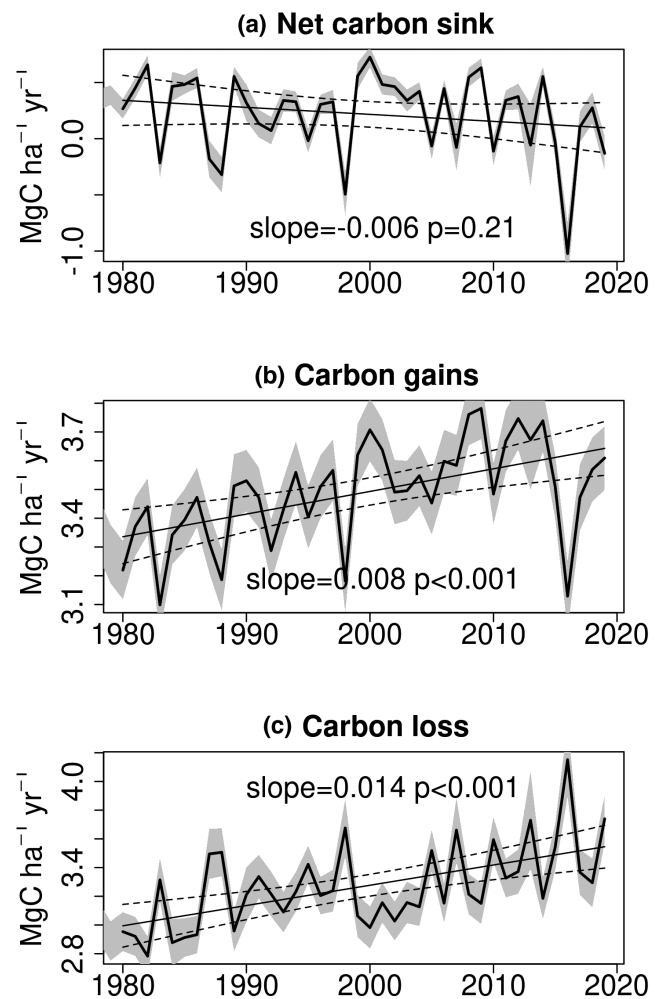

FIGURE 2 Long-term carbon dynamics of rainforest over the Amazon basin. (a–c) Trends in net aboveground biomass carbon sink (a), carbon gains from tree growth (b), and carbon losses from tree mortality including both self-thinning and drought-induced tree mortality (c). The continuous lines indicate the modelled forest carbon dynamics in Amazonia and the shading area corresponds to the 95% confidence interval. Slopes and *P* values are from linear regression models.

non-modeled biotic disturbances. Yet, it is encouraging to see that the essential signal of a decelerating biomass sink from increased mortality is captured by our simulations.

3.2 | Biomass growth and mortality for the recent droughts, and sensitivities to water deficits

3.2.1 | Mean biomass gains and losses during normal years

During the 2000s, excluding the 2005 and 2010 droughts to focus on non-drought periods, forests gained AGB, at a rate of +0.44 MgC ha^{-1} year^{-1} (95% confidence interval 0.39–0.50 Mg C ha^{-1} year^{-1}), that is, they acted as a carbon sink in biomass. The total carbon sink was 0.22 Pg C year^{-1} over our intact forest area of 500 Mha. There were significant differences among the four regions (tested from the Tukey HSD post-hoc test; Figure S1). We found a higher net AGB sink density in the Western Amazon (+0.69 Mg C ha^{-1} year^{-1}), followed by the Guiana Shield (+0.41 Mg C ha^{-1} year^{-1}). The gross gain in AGB, due to growth alone, was 3.6 Mg C ha^{-1} year^{-1}, with the highest gross gain in the Guiana Shield (+4.2 Mg C ha^{-1} year^{-1}). The gross loss in AGB was also highest in the Guiana Shield, and lowest in the Western Amazon. A 'high-gain,

high-loss' pattern, thus a larger turnover, was modelled in the Guiana Shield region.

3.2.2 | The 2005 drought

This event has its severity epicenter located in the Western Amazon, as seen from Z-transformed MCWD (Figure 3). In this epicenter, we simulated a larger net AGB loss (–0.6 Mg C ha^{-1} year^{-1}) than for the rest of the Amazon. The net annual loss from October 2004 to September 2005 was driven by a decline in growth and an increase in mortality (Figure 3), consistent with forest plots evidence shown by Phillips et al. (2009). The most severe water deficit matched the largest loss of AGB in our simulations. In the Western Amazon, we found a 2.0 Mg C ha^{-1} (95% CI: 1.5–2.5) net loss of AGB relative to non-drought condition (Table S1). This net loss is composed by a modest decrease of growth gain of 0.2 Mg C ha^{-1} (95% CI: 0.1–0.3) and a large increase of mortality loss of 1.8 Mg C ha^{-1} (95% CI: 1.2–2.3). These figures are comparable with plot data analysis by Phillips et al. (their fig. 2).
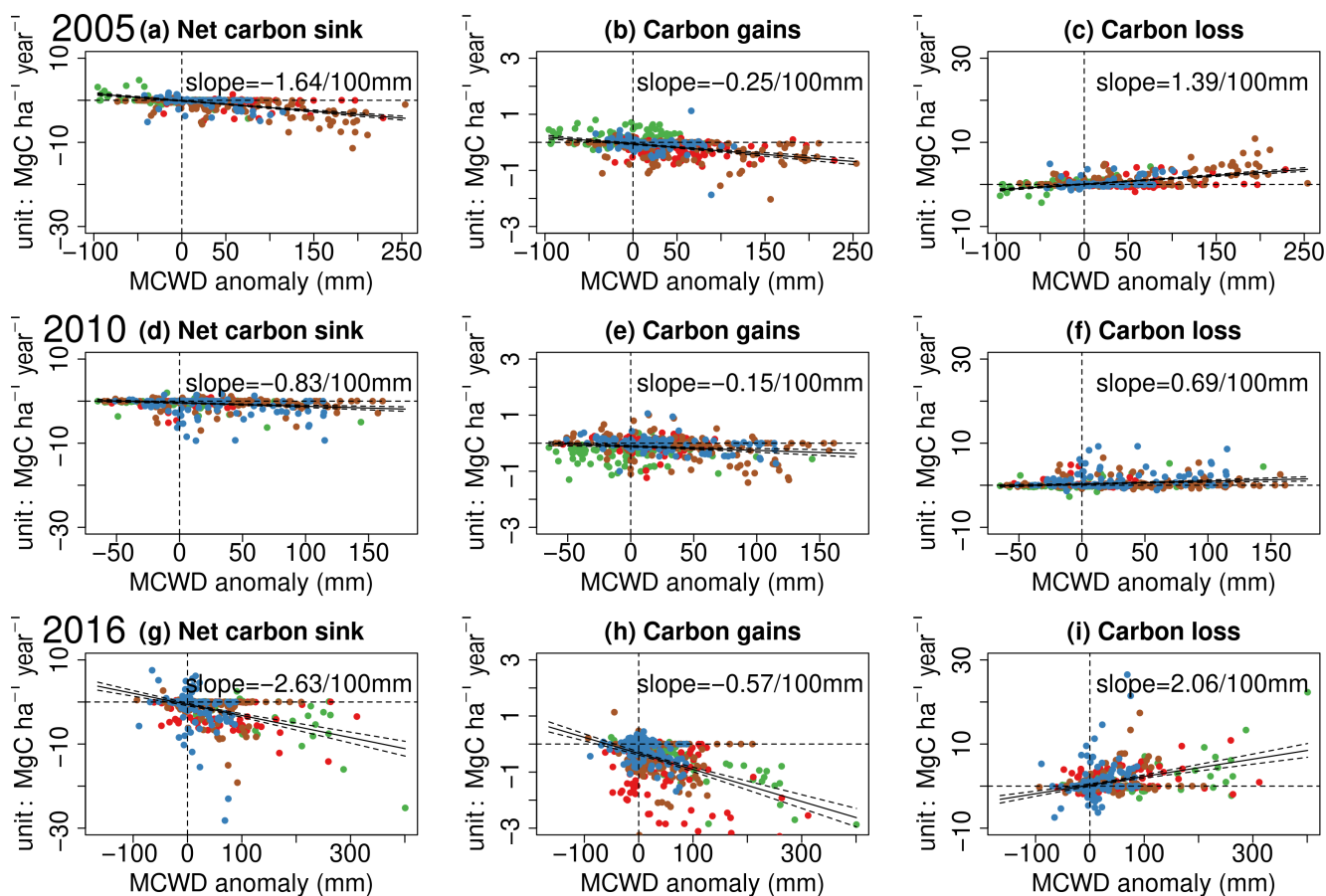
FIGURE 3 AGB versus drought severity in (a–c) 2005, (d–f) 2010, and (g–i) 2016. Severity is defined from MCWD, with higher positive values denoting more acute water stress. The color of the points corresponds to four regions, red: Guiana Shield, green: East-Central Amazon, brown: Western Amazon, and blue: Brazilian Shield. The first column (a, d, g) gives the net AGB sink anomaly with MCWD. The second one (b, e, h) the AGB growth gain anomaly. The third one (c, f, i) the AGB loss (mortality) anomaly. Map lines delineate study areas and do not necessarily depict accepted national boundaries.

3.2.3 | The 2010 drought

This event was most severe in the north of the Brazilian Shield. According to our climate forcing data (CRUJRA), the drought severity, however, was lower and the affected area was smaller than for the 2005 drought, as shown by the magnitude of MCWD anomaly, which spans over −100 to 150 mm (Figure 3). The drought severity and impacted area in 2010 are a bit different than in Lewis et al. (2011), due to different rainfall forcing data (TRMM satellite rainfall data in Lewis et al., 2011 vs. CRUJRA in our study). The drought sensitivity of the AGB net change to MCWD was lower in 2010 than in 2005 (0.83 vs. 1.64 MgC ha^{-1} per 100 mm MCWD) over whole basin but comparable in their epicenters (Table S1). Yet, like for the 2005 event, the effect of the drought on net AGB change was dominated by higher AGB loss and a relatively modest reduction of AGB gain.

3.2.4 | The 2015/16 El Niño drought

This event is mainly centered in northeastern Amazonia (Guiana Shield). The simulated response of AGB is shown in Figure 3g–i. The magnitude of the MCWD anomaly shows that this drought was more severe than the two previous events. Therefore, we found a higher ΔAGB sensitivity (Figure 3g–i, Figure S2) of −2.63 MgC ha^{-1} per 100 mm MCWD than in the former two droughts. Furthermore, the

AGB gain sensitivity was of −0.57 MgC ha^{-1} per 100 mm MCWD, in smaller magnitude than the sensitivity of AGB loss of 2.06 MgC ha^{-1} per 100 mm MCWD. In addition, for a 100 mm increase in MCWD, we simulated in 2015/16 an increase of 12 days as 'mortality risk', and a 1.2% increase in the annual mortality rate compared with the baseline period (Figure S3). In the northern Brazilian Shield epicenter, we simulated a greater AGB loss and a higher stem mortality rate even in pixels where MCWD anomaly remained below 100 mm. This response likely reflects other stress factors causing an increase of transpiration, followed by loss of conductance and mortality in our model, especially high temperature and elevated vapor pressure deficit (VPD).

3.3 | Drought severity and biomass loss for the most severe drought events of the past century

After having shown that the simulated sensitivities of growth and mortality to MCWD compared well with forest plots data (at least for the 2005 event that was extensively measured across many plots), we now turn to the analysis of AGB deficits during the most severe droughts of the last century (1916, 1926, 1963, 1983, 1998, 2005, 2010, 2016). Figure 4 shows the spatial distribution of the drought intensity, that is, the Z-score of MCWD anomalies (Section 2.3). The epicenter of different droughts varied across events. The northwest Amazon 'ever-wet' region was rarely affected. The northern Brazilian
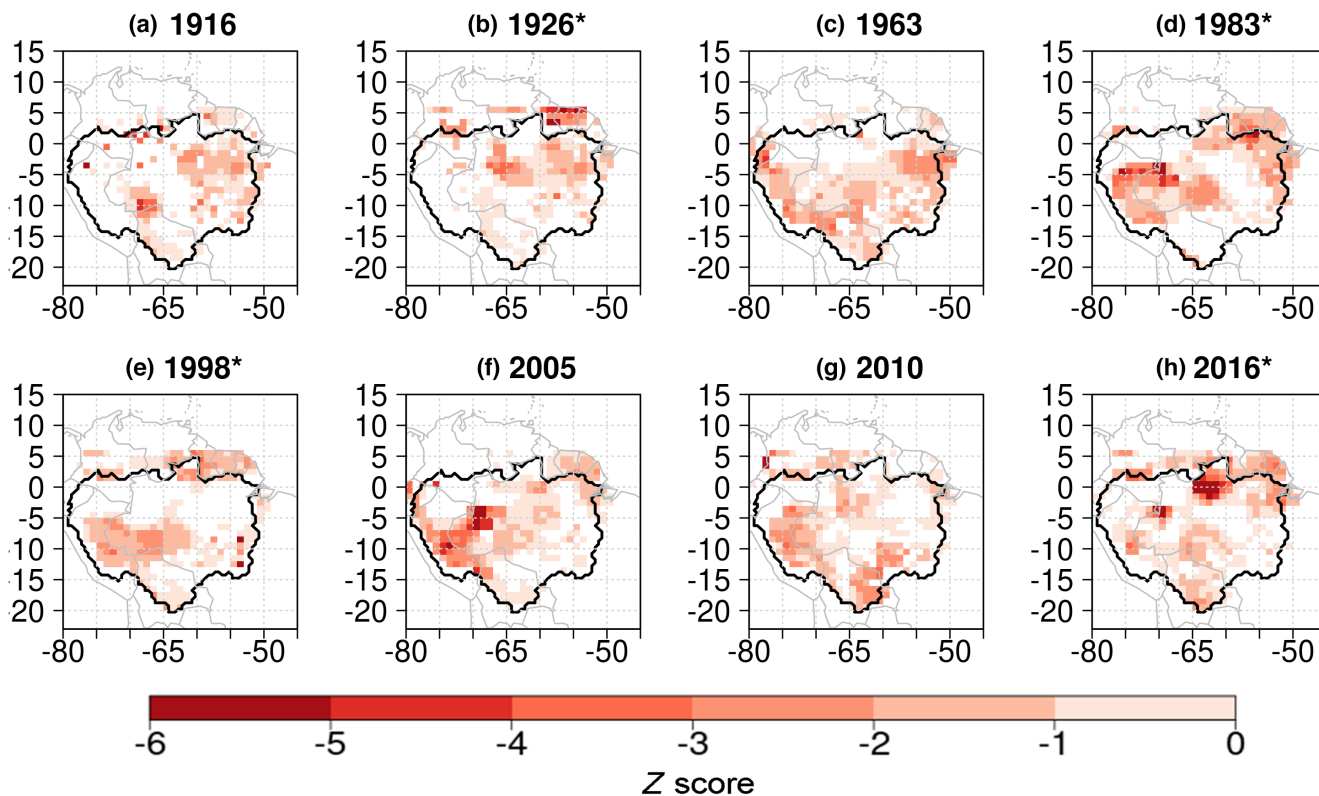

FIGURE 4 Spatial distribution of the drought intensity of the top most severe droughts since 1901, is assessed by Z-score values of maximum climatological water deficit anomalies relative to their decadal baseline.

Shield, also an 'ever-wet' region where the dry season even sees a periodical increase of GPP (Green et al., 2020), was particularly affected by the 2015/16 El Niño drought. The southwest regions were hit by the 1983 and 2005 droughts. The East and northeast regions were affected by the 1916, 1983 and 2015/16 droughts. The Southern Amazon was affected by the 1963 and 2010 droughts.

3.3.1 | The largest droughts of the century compared for their area exposed to different drought intensities and area of AGB loss

Figure 5 shows the number of 1° pixels for different severity classes (Z-scored CWD). The 2015/16 drought is clearly ranked as the most severe event on record, followed by 1983 and 2005. Both the area under drought (negative Z-score), representing 63% of the evergreen forest area, and the area under *extreme* drought, show the largest values during the 2015/16 event. Mirroring mainly the spatial patterns of water deficit, the net AGB dynamics from our simulation is shown in Figure 6. Outside the epicenter of each drought, ΔAGB was small and positive (Figure 6) indicating a continuous long-term carbon sink (Figure 2). In the drought affected pixels, we found that the AGB net losses always ranked with the severity of drought. For instance, ΔAGB in 2010 was less negative than that during the more extreme droughts of 2005 and 2016 (Figure 6). Among the top 8 drought events of the last century, we found differences in the fraction of area with negative ΔAGB at a given level (Figure 7, Figure S4). The area showing negative ΔAGB values was the largest in the 2015/16 El Niño, followed by the 1983 one. The area with the most negative

ΔAGB per unit area (e.g., a loss more than 6 MgC ha^{-1} year^{-1}) was the most extensive in 2016, followed by 1983 (Figure 6).

3.3.2 | Wet-season droughts caused larger AGB loss than dry-season ones

We investigated the differences in AGB responses between wet-season and dry-season droughts, distinguished by their DTI index (see Section 2.3 and SI Notes S1). It should be noted that the 'wet-season' drought actually happened during the period that was normally the wet season but encountered a severe water deficit, which can be regarded as the extension of dry-season length or severity. From Figure 8, we can see that the east-central Amazon region which has a low rainfall seasonality, shows DTI > −0.2 in 1983 and 2016. In other words, these two drought events appeared in the wetter quarter of the year, and can be deemed as wet-season droughts. DTI values close to −1 in the southwest Amazon in 2005, implies this event was a clear dry-season drought. The epicenters of the 2010 drought are more diffuse and show DTI values between −0.2 and 0.2, which makes this event a composite of dry and wet season drought. As the intensity of wet-season and dry-season droughts differs, so does the corresponding AGB dynamics. Figure 5 shows that the drought severity was higher in the wet-season droughts of 2016 and 1983, and that the drought exposed area was also higher during these two events. Figure 7 shows that the AGB loss differs between wet- and dry-season droughts. Namely, the area undergoing large AGB loss is larger for wet-season droughts like 2016 than for dry-season droughts like 2005 (Figure 7). Moreover, if we compute the mean ΔAGB corresponding to different Z-score levels, we found
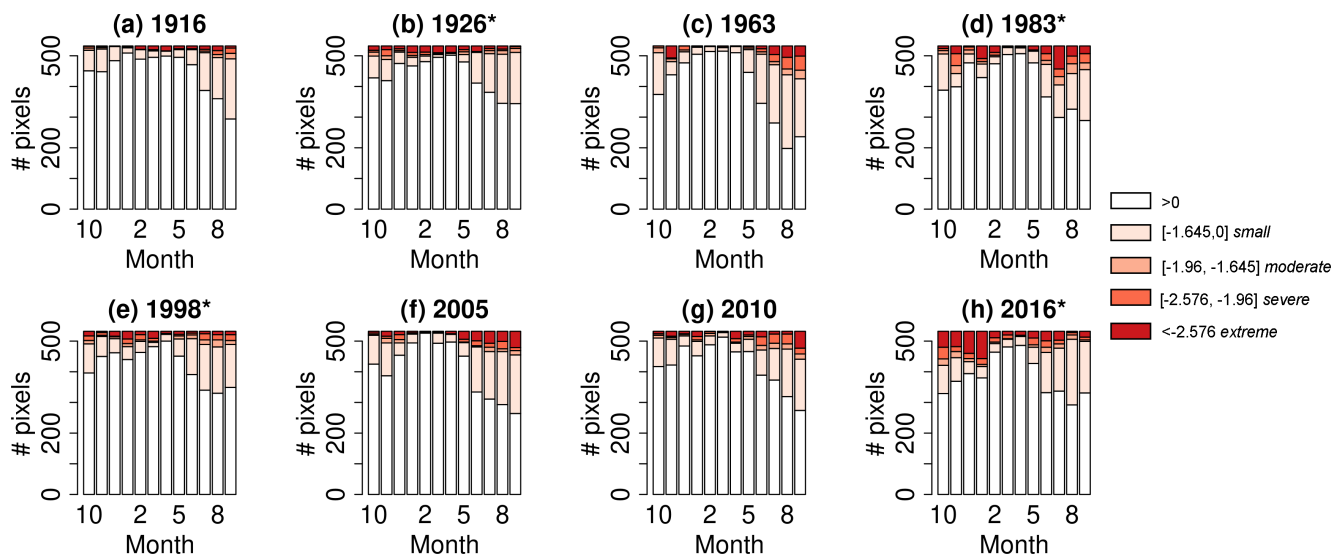
FIGURE 5 Frequency distribution of different drought intensity classes (Z-score of monthly climatological water deficit (CWD) corresponding to increasing severity). The thresholds of −1.645, −1.96, and −2.576 correspond to 90%, 95%, and 99% confidence intervals of the distributions, respectively. The asterisks in the title of a panel indicate an El Niño drought (wet-season drought). The # pixels on the vertical axis means the number of 1° model pixels with CWD values in each interval.

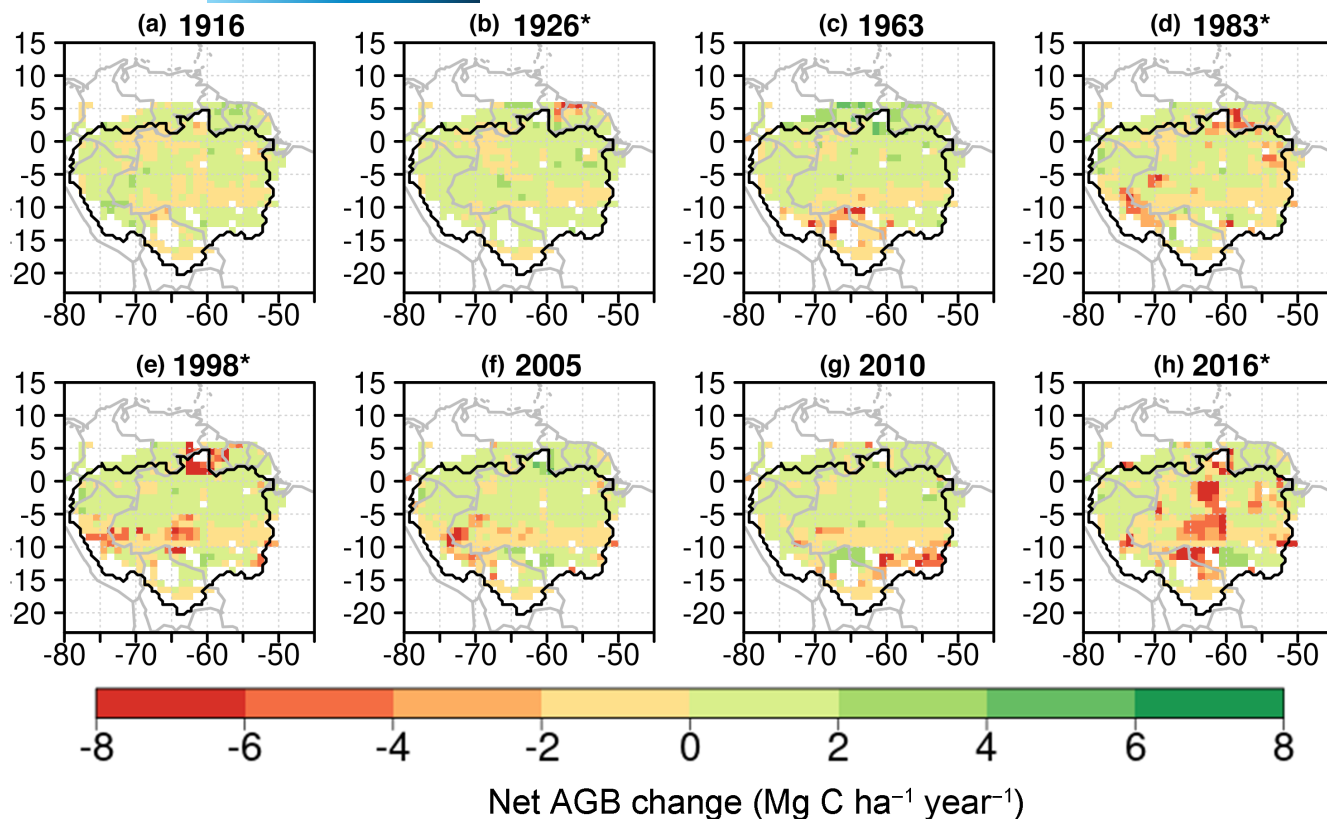**FIGURE 6** Spatial distribution of the simulated net AGB change during the eight largest drought events since 1901. Such change is calculated on yearly interval, from the October in the previous year to September in the current year. The asterisks in the title of a panel indicates an El Niño drought. Negative value denotes carbon sources and positive value means carbon sink. Map lines delineate study areas and do not necessarily depict accepted national boundaries.
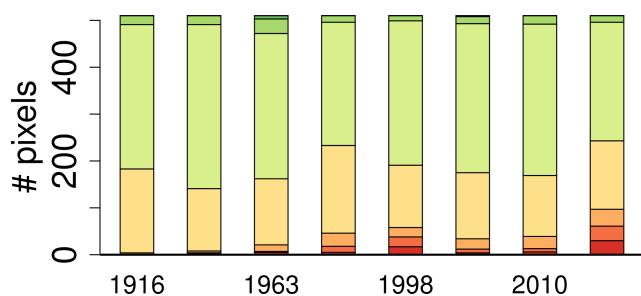

FIGURE 7 Regional extent of net AGB change during eight drought events. The colors correspond to the different levels of net AGB changes with the same color palette than in Figure 6. # pixels means the number of 1° model pixels that underwent net biomass carbon change in each interval.

that the mean ΔAGB is always the most negative during (El Niño) wet-season droughts, no matter which Z score level is considered (Table S2).

3.3.3 | The last 20 years show the largest AGB loss caused by droughts

We then compared drought effects on AGB on decadal-scale. To do so, we calculated the cumulative AGB loss in successive 20-year

intervals since 1901 (Figure 9). Looking at the three extreme drought events in the last 20-year, it is clear from our simulations results that the cumulative AGB loss over this period was higher than during any other previous 20-year interval since 1901 (Figure S5). The region which had the higher level of AGB loss (>4 Mg C ha^{-1} year^{-1}) during the last 20 years is the East-central Amazon, even though this region was rarely affected by previous droughts.

3.4 | Interactions between drought and elevated CO_2

We make the reasonable hypothesis that (in the model) elevated CO_2 induces stomatal closure and should, thus, partly alleviate the negative effect of drought on AGB. To assess the extent to which the drought effects can be alleviated, we separated the effects of climate change alone vs. increased CO_2 concentration during the major droughts of the last Century through factorial simulations (S1–S3 see Section 2.2). The results are shown in Figure 10. The simulation S2 driven by observed historical climate (including the eight drought events studied above) and atmospheric CO_2 increase, while S1 was driven by recycled 1901–1920 climate (no climate change), and S3 used historical climate but maintained the CO_2 concentration constant at 296 ppm (no CO_2 increase). The comparison between S1 and S2 shows that historical
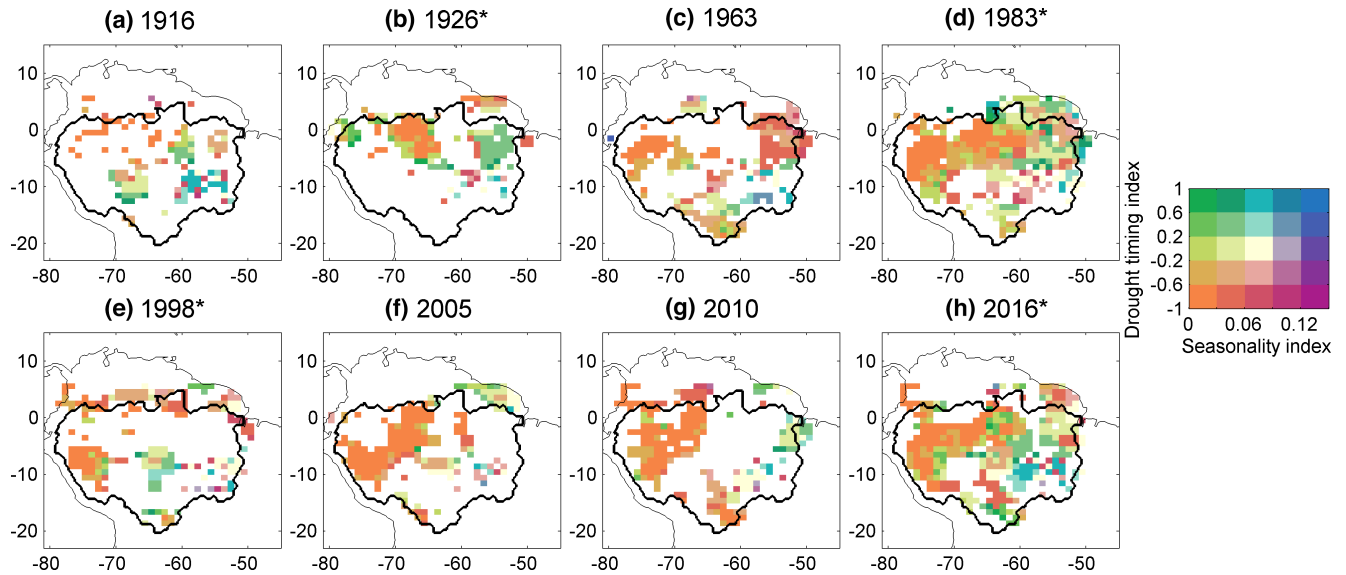
FIGURE 8 Bivariate plots showing the spatial pattern of the rainfall seasonality index and drought timing index (DTI) in the Amazon for the eight largest droughts since 1901. Negative values of DTI mean that drought with the most negative Z-score of rainfall anomaly happens in the drier months of the year. Only pixels with a drought Z-score of MCWD below −1.645 are shown, which is at least a *moderate* drought (see definition of drought intensities in SI). The asterisks in the title of each panel indicates an El Niño drought. Map lines delineate study areas and do not necessarily depict accepted national boundaries.
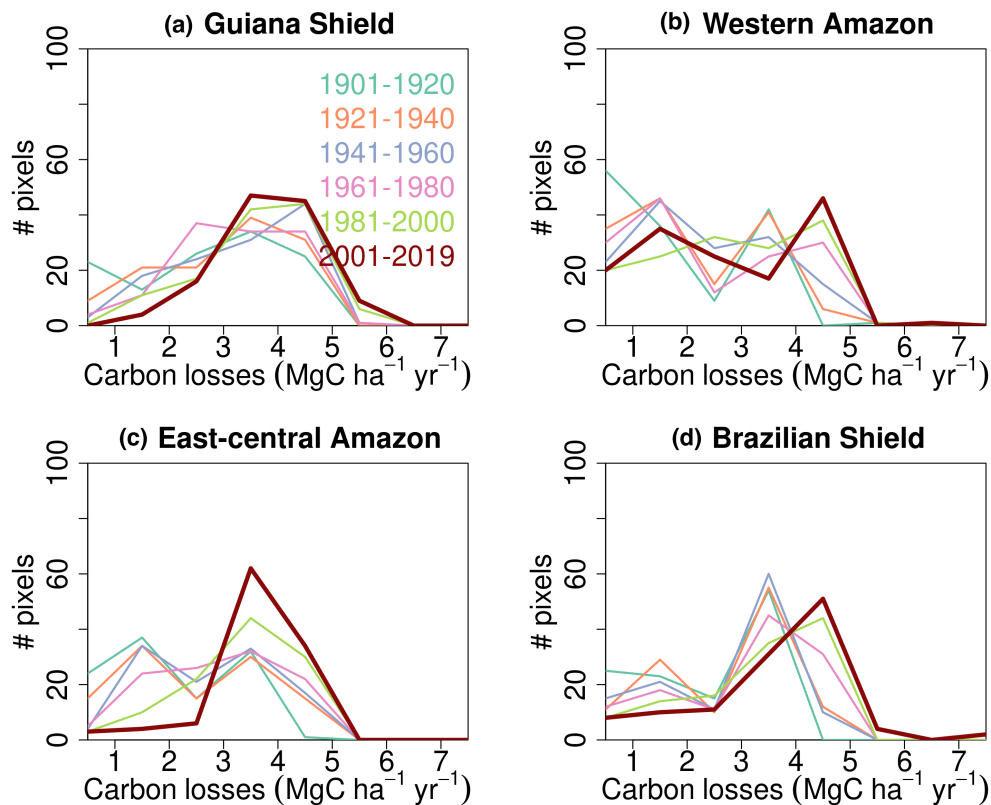
FIGURE 9 Comparison of cumulative AGB loss in 20-year intervals in different regions since 1901. # pixels means the number of pixels underwent carbon loss in each interval. The last 20-year period is highlighted as the thick red line.

climate change since 1901, that is, mainly droughts, has suppressed plant growth and increased mortality losses. The net biomass carbon gains during each drought year are, thus, lower in S2 than in S1.

The comparison between S2 and S3 allows us to isolate the effect of rising CO_2 concentration. The AGB gain was significantly higher under S2 than S3 ($p < .05$), because of the increase of NPP from

FIGURE 10 AGB gain from growth, loss from mortality and net AGB change in the epicenters of each major drought from the three scenarios. S1: Varying CO_2 and recycling climate over 1901–1920, S2: Varying CO_2 and historical climate change, S3: Historical climate change and constant CO_2 concentration. The epicenter of a drought is defined by pixels with Z-scored MCWD below −1.645, corresponding to 90% confidence interval following normal distribution.
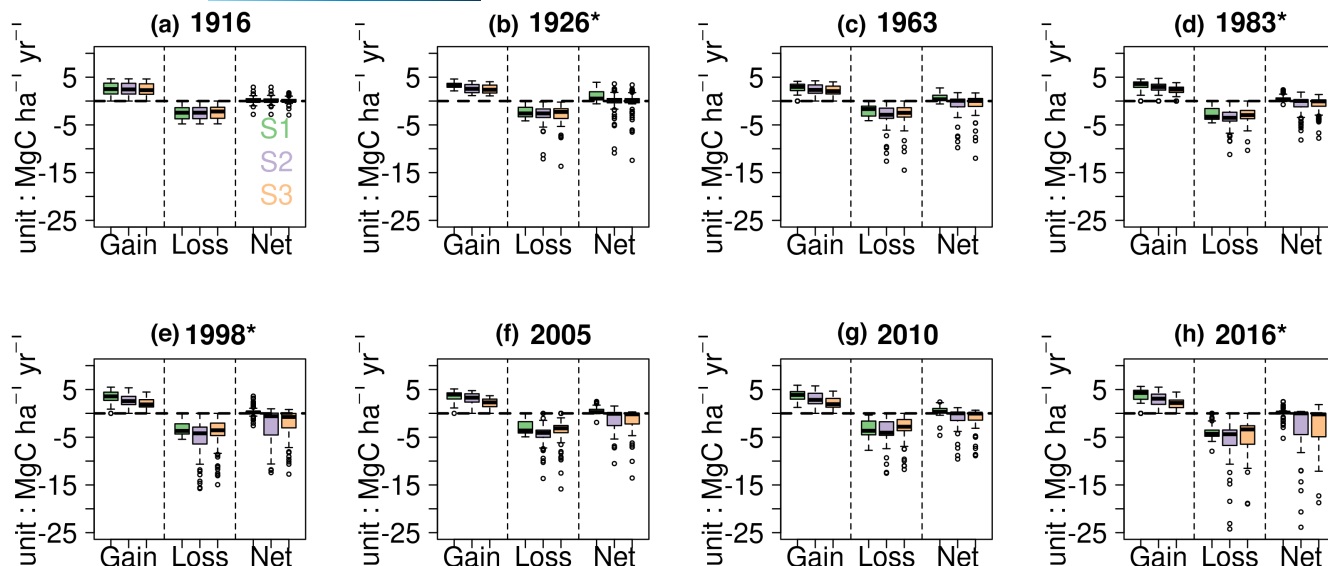
elevated atmospheric CO_2. The AGB density was higher in S2 than in S3, reflecting a higher carbon accumulation due to the historical increase of CO_2 (Figure S6). Yet, there was also significant difference of AGB loss between S2 and S3 ($p < .05$). When we look at the mortality risk with and without rising CO_2, in the epicenter of the eight drought events (Z-score of MCWD below −1.645), the number of days with mortality risk was significantly higher in S3 than that in S2, with a difference that can reach up to 10 days (Figure S7). This result implies that, in our model, elevated CO_2 induced a partial alleviation of moisture stress from stomatal closure and reduced transpiration, offsetting a possible increase of transpiration due to higher foliage area. During droughts, the modeled evapotranspiration rate confirms a smaller soil moisture stress in S2 (Figure S8) compared with S3 where CO_2 is fixed. Since the model here did not include the downregulation of nutrient limitation, the CO_2 fertilization effects could be overestimated.

4 | DISCUSSION

4.1 | Mortality in the model and its sensitivity to water deficits

4.1.1 | Mean patterns of mortality and turnover

A clearer understanding on the response of the Amazon rainforest to drought is indispensable for future predictions. We found that our model, despite having its parameters calibrated only for the Caxiuanã throughfall experiment, and lacking a description of the diversity of plant traits, is capable to produce realistic average cross-basin mortality rates, and higher mortality rates and biomass losses in the epicenter of each drought. With our hydraulic

failure—mortality module adding up to background tree mortality (from self-thinning), our simulations (Figure S9) of the mean spatial pattern of mortality are comparable with mortality rates from inventory data shown by Esquivel-Muelbert et al. (2020). Namely, there is a prevalence of higher average mortality in the Brazilian Shield. Nevertheless, the average pattern of 'high-gain, high-loss' observed in the Amazon, for example, by Hubau et al. (2020) is not captured by our model. Plot observations suggest a larger turnover (larger gain and loss fluxes) in the Western Amazon, possibly due to different species composition reflecting adaptation to more fertile soils near the Andes (Yang et al., 2014). Our model simulates in contrast a pattern of 'high-gain, high-loss' in the Guiana Shield region. This can be related to the fact that our model lacks representations of nutrient dynamics (higher phosphorus content of soils promoting growth in the Western forests) and species traits regional differences, and that it includes only drought mortality and not the other disturbances modulating forest turnover, like windthrown in the Western Amazon (Negrón-Juárez et al., 2018).

4.1.2 | Drought impacts on demography

The hydraulic architecture and drought induced mortality scheme on top of the demography structure permit us to analyze the tree mortality rate per tree size. Besides the smallest tree size cohort, the annual mortality rate increases with tree size in our simulations, especially in area with a moderate drought risk (Z-score MCWD < −1.645) as shown in Figure S10. A larger mortality of taller trees is independent of the region considered, since greater gravitational energy is required to pull water upward along longer transport pathways in bigger trees in the model. Monitoring of forest plots

showed that older or larger trees were disproportionally threatened by El Niño drought (Meakem et al., 2018). However, field measurement evidences have not reached consensus as they showed vulnerability of bigger trees (Bennett et al., 2015) or no mortality-size relationship (Powers et al., 2020), where the size dependence could be superseded by hydraulic safety traits that can be more prevalent at coarser scales, as well as the agreement regarding whether within-species covariation between tree size and water availability holds at species or landscape level has not been obtained (Trugman et al., 2021). To compare model results with inventories that only sample trees larger than 10 cm, we only looked in the model at growth in corresponding cohorts. With regard to the recruitment, we simulated more new individuals recruited during drought than non-drought period (Figure S11), since the recruitment rate is parameterized in relation to LAI (Joetzjer et al., 2022). In other words, a decrease of LAI promoted recruitment during drought in our simulations.

4.1.3 | Sensitivity of biomass to droughts compared with observations

The drought sensitivity simulated by our model shows an emerging positive relationship between mortality and water deficit. This result is consistent with forest plot observations. The simulated drought sensitivity is comparable with the one observed in inventory data for the 2005 drought (Phillips et al., 2009). Inventory measurements did not sample the epicenter of the 2010 drought. Unlike for the 2005 event, however, selected plots were measured shortly after 2010, thus reducing possible confounding effects of post-drought climate conditions. These scarce data indicate that forest sites that were experiencing a severe drought gained less biomass in 2010 but showed no evidence for a significant mortality co-variation with drought severity (Feldpausch et al., 2016). During the 2010 drought, data from other sites with regular measurements of ecosystem-level fluxes (Doughty et al., 2015) showed that foliage and woody NPP remained unchanged at wet lowland sites, although autotrophic respiration (Ra) decreased. In the 1° grid cells containing the sites of Doughty et al., we modeled a decreasing GPP, NPP and Ra with increasing MCWD (Figure S12), which is inconsistent with Doughty et al. (2015), excepted for Ra. Our model may over-estimate the negative response of GPP and NPP to drought at these sites, possibly because some of the sites include forests that had access to ground water, a process ignored in the model. It is also possible that soil properties in the 1° grid cells do not correspond to those observed at the sites. When we combined the three most recent drought events together and divided MCWD anomalies into distinct severity classes, we found that the negative response of AGB from mortality increases above a threshold of 50 mm MCWD anomaly (Figure S13). Besides, several pixels with a positive MCWD anomaly show only a small ΔAGB. For such 'insensitive pixels' both plant hydraulic architecture and soil hydraulic properties seemed to control plant water availability and biomass dynamics. We note here that our model was calibrated against the Caxiuanã experiment with a half-exclusion of rainfall alone and no coincident manipulation of temperature, and it could underestimate the sensitivity of AGB to compound events with low rain, high temperature, and high VPD.

4.1.4 | Importance of soil texture for modeling mortality during drought

In the model, a rainfall deficit alone does not always bring severe water stress and mortality as shown in the previous paragraph. This model behavior is dependent on soil texture parameters. Soils with a higher clay content are closer to their wilting point when rainfall decreases but have a greater soil water-holding capacity (difference between field capacity and wilting point) (McCulloh et al., 2019). Levine et al. (2016) found that water stress in soils with higher clay content is likely to influence more negatively plant biomass dynamics. Our simulations used the HWSD soil texture map (Wieder et al., 2014) which has loam distributed in the Western Amazon, and silt loam and sandy clay loam soils in the central Amazon. Although this soil texture map produces a reasonable mean mortality rate, there are 'insensitive' pixels where PLC remains below the threshold of 50% (inducing mortality) even under a severe water deficit (see Figure S14). Using a more clay rich soil texture in the model could produce a more sensitive response of AGB to water availability, and give results more comparable with local inventory observation. As a test of this hypothesis, at one pixel in the East-Central Amazon, we prescribed a *sandy clay* texture instead of *loam*, and found that climate-induced mortality increased a lot in 2005, and AGB became more sensitive to MCWD with sandy clay. The spatial variability of soil properties is high, including at small scale (Marthews et al., 2014). Therefore, the mismatch between site-specific soil texture and our 1° model pixels should be considered to understand the model-observation misfit.

4.1.5 | Importance of threshold parameters that trigger mortality from hydraulic failure

With regard to the sensitivity of mortality to tree conductance loss (PLC) in each cohort, the drought exposure threshold and the mortality rate applied to kill trees exceeding the exposure as defined for simulating mortality by Yao et al. (2022) are coupled in our model. Adjusting the exposure threshold of PLC causing drought-induced 'cavitation' mortality in the model is difficult, since there is almost no measurement for tropical trees that monitored impairment and mortality risk above a critical PLC threshold. Critical PLC thresholds strongly depend upon species, related to traits like height or wood density. For example, Brodribb et al. (2020) found that a vulnerable tall tree died in 1 week after reaching cavitation. We, thus, would need field-based measurement of hydraulic damage in the tropics to better constrain the drought exposure threshold parameterization of the model.

4.2 | Perspective to reduce uncertainty of the biomass drought sensitivity

4.2.1 | Variable hydraulic traits

The drought sensitivity of AGB in the real world relates to the diversity of hydraulic traits. Those traits confer regional variations in drought tolerance, and associate with habitat preferences (Kunert et al., 2021), although some traits could be spatially coherent (Powell et al., 2017). Our study used a set of hydraulic parameters for traits calibrated from the Caxiuanã drought experiment. In reality, there is a broader diversity reflecting plant water use strategies, even at small spatial scale. Highly variable water potentials at which 50% of conductivity is lost (Ψ_{50}) in stem xylem were observed by Oliveira et al. (2019). Species traits spatial differences in water deficit *affiliation*, that is how traits leading to hydraulic failure have adapted to local long-term frequency and severity of drought at a given place, also relate to mortality risk. But a high *affiliation* to drought does not warrant resistance to the more severe 'new types' of drought emerging in the recent years (Esquivel-Muelbert et al., 2017). Apart from background climate affiliation, hydraulic traits also vary with tree size (Bittencourt et al., 2020), soil fertility and topography (Oliveira et al., 2019). Below, we discuss a few critical traits that could be given spatial variability in our model.

4.2.2 | Tree water potentials safety margin

Hydraulic safety margins calculated as the difference between Ψ_{50} and the minimum water potential during a drought correlates with mortality risk among species (Powers et al., 2020). Larger hydraulic safety margins protect trees from hydraulic damage (Ziegler et al., 2019). Interspecific heterogeneity in hydraulic performance for xylem safety and efficiency trade-off should give the possibility to see a possible dominance of drought-tolerant species in the case of more frequent and severe droughts (Zuleta et al., 2017). To capture these effects in models, we see a critical need for incorporating functional diversity in the traits that determine vulnerability and water regulation strategies (Anderegg et al., 2019). Liu et al. (2021) proposed to constrain indirectly the distribution of plant hydraulic traits with satellite observations of VOD, evapotranspiration and soil moisture. This approach could provide useful insights about hydraulic traits such as water potential safety margin and pre-dawn water potential by calibrating optimal parameters in the model to minimize the difference between satellite observations and simulations.

4.2.3 | Wood density

Wood density is partly related to stem water potentials, life history and drought resistance (De Guzman et al., 2021). Species with low wood density are expected to be more vulnerable to droughts. On the contrary, species with high wood density are considered to be more resistant to hydraulic failure, as evidenced by negative effect of wood density on mortality in response to the 2010 drought through generalized linear mixed model (Zuleta et al., 2017). Besides wood density, trade-off in wood volume allocation also relates to xylem efficiency-safety trade-off (Janssen et al., 2020). Site-level evidence showed that easily measured traits like wood density can help to understand drought responses (Santiago et al., 2018). In other words, through the measurement of wood density, and its relationship with plant inherent hydraulic traits, for example, the negative linear relationship between sapwood turgor loss point and wood density found by De Guzman et al. (2021), variability of hydraulic parameters could be incorporated into our model using new wood density maps (Mitchard et al., 2014).

4.3 | Reducing uncertainty on the effect of elevated CO_2 to alleviate trees' response to drought

For predicting biomass dynamics in Amazon rainforests, interactions between drought and elevated CO_2 are of key importance. Our model produced a higher AGB gain under elevated CO_2 during droughts but this positive effect was overall offset by negative climate effects, as shown in Figure 10. The positive effects on growth from elevated CO_2 in our model is spatially uniform, while there is spatial heterogeneity in the AGB loss response to drought. During drought years, most pixels show a lower mortality risk in S2 with elevated CO_2, compared with S3 with fixed CO_2 (Figure S7), consistent with simulations from (less advanced) terrestrial biosphere models showing that CO_2 fertilization decreased the probability of dieback in eastern Amazon (Zhang et al., 2015). Reduced transpiration due to increased CO_2 (a difference between −0.4 and 0mm/day from S2 − S3) was modeled in most pixels, for example during the 2015/16 event (Figure S8). Yet, this response of transpiration to increasing CO_2 is not spatially uniform and has uncertainties (Mengis et al., 2015). The degree to which water stress can be mitigated by rising CO_2 needs further calibration, for example, through field-studies of leaf hydraulics adjustment (Cernusak et al., 2013; Zuidema et al., 2020). New data such as the future Amazon Free-Air CO_2 enrichment experiment, should also help resolve the optimal stomatal behavior from the trade-off between carbon uptake and water loss. We should also notice that the nutrient cycles are not well characterized in current model version, where the nutrient limitation like N and P deficit can modify the response of vegetation to increasing CO_2.

4.4 | Legacy mortality and post-drought biomass recovery

4.4.1 | Legacy mortality

Besides hydraulic transport recovery, legacy effects of drought have an impact on living trees through partial damage. For example,

elevated post-drought mortality was shown in the Colombian Amazon (Zuleta et al., 2017) and also central Amazon (Aleixo et al., 2019). Currently, our model only considers cumulative drought exposure through PLC and has no legacy mortality effects. Such carryover effects could be further incorporated. For example, we may calibrate the depletion of labile carbon pools and reserves (already included in the model) after a drought to investigate how nonstructural carbohydrate (NSC) change during the drought and whether less available NSC would affect the following growth trajectory (Signori-Müller et al., 2021). Furthermore, increased mortality during drought is also linked with the appearance of other disturbances, like fire and insect outbreaks (Brando et al., 2014), since droughts concur with peaks of fire activity. Thus, interaction with other disturbances, which can induce a 'death spiral' (Franklin et al., 1987), also needs to be considered. For example, we could adapt the fire module (Yue et al., 2014) of ORCHIDEE to reproduce Amazon fires, through which the effects of droughts and the accompanying higher fire risks can be tracked.

4.4.2 | Post-drought resilience

In addition to distinct resistance strategies, possible recovery processes after embolism are also crucial in the simulation of hydraulic efficiency-safety trade-offs (Klein et al., 2018). Recovery from hydraulic damage like embolism repair or vessel refilling can buffer drought mortality. After reaching the cavitation threshold, to what extent the embolism reversal can happen after the re-watering and how much xylem tension can relax are still under debate and require more evidences, like the experiments of the dry-down and re-watering on plant individuals that can permit the detection of the plant tolerance to water stress condition and their recovery abilities, to enable a generalized parameterization into process-based models.

5 | CONCLUSION

We used a process-based model describing plant hydraulics, background light competition and drought induced tree mortality, ORCHIDEE-CAN-NHA, to evaluate the drought sensitivity at regional level and investigate AGB changes for the eight most severe drought events since 1901 over the Amazon. The model can successfully quantify the drought sensitivity of AGB growth and mortality to cumulative water deficits compared with plot data collected for the 2005 and 2010 droughts. We assessed a higher sensitivity of net AGB change in response to water stress during the extreme 2015/16 drought. Comparison of extent and severity of the eight droughts and their AGB anomalies indicates that the 2015/16 event was the most severe both in terms of drought intensity in its epicenter and the area where severe biomass loss occurred. Factorial simulations helped us to discern the contribution of climate change and increased CO_2 concentration: climate change negatively affected AGB gain and loss, whereas moisture stress was reduced to some extent by elevated CO_2. More field-evidence, like hydraulic

traits distributions and a better accounting of soil texture heterogeneity, are priorities to fill the model-observation gap and produce more reliable spatial gradients of mortality risk. We hope that this study makes an important step forward in quantifying the large-scale carbon impacts of tropical forest drought and enhances our ability to make future predictions.

AUTHOR CONTRIBUTIONS

Philippe Ciais and Yitong Yao designed the study. Yitong Yao ran the simulation, analyzed the outputs and drafted the manuscript. All authors contributed to manuscript drafts, where Philippe Ciais substantially contributed to the final manuscript.

CONFLICT OF INTEREST

The authors declare no conflicts of interest.

ORCID

Yitong Yao https://orcid.org/0000-0002-1713-6719
Philippe Ciais https://orcid.org/0000-0001-8560-4943
Nicolas Viovy https://orcid.org/0000-0002-9197-6417
Emilie Joetzjer https://orcid.org/0000-0001-6781-1535
Jerome Chave https://orcid.org/0000-0002-7766-1347

REFERENCES

Aleixo, I., Norris, D., Hemerik, L., Barbosa, A., Prata, E., Costa, F., & Poorter, L. (2019). Amazonian rainforest tree mortality driven by climate and functional traits. *Nature Climate Change*, 9(5), 384–388.

Anderegg, W. R., Anderegg, L. D., Kerr, K. L., & Trugman, A. T. (2019). Widespread drought-induced tree mortality at dry range edges indicates that climate stress exceeds species' compensating mechanisms. *Global Change Biology*, 25(11), 3793–3802.

Bennett, A. C., McDowell, N. G., Allen, C. D., & Anderson-Teixeira, K. J. (2015). Larger trees suffer most during drought in forests worldwide. *Nature Plants*, 1(10), 15139. https://doi.org/10.1038/nplants.2015.139

Bittencourt, P. R., Oliveira, R. S., da Costa, A. C., Giles, A. L., Coughlin, I., Costa, P. B., Bartholomew, D. C., Ferreira, L. V., Vasconcelos, S. S., & Barros, F. V. (2020). Amazonia trees have limited capacity to acclimate plant hydraulic properties in response to long-term drought. *Global Change Biology*, 26(6), 3569–3584.

Brando, P. M., Balch, J. K., Nepstad, D. C., Morton, D. C., Putz, F. E., Coe, M. T., Silvério, D., Macedo, M. N., Davidson, E. A., & Nóbrega, C. C. (2014). Abrupt increases in Amazonian tree mortality due to drought–fire interactions. *Proceedings of the National Academy of Sciences of the United States of America*, 111(17), 6347–6352.

Brienen, R. J., Phillips, O. L., Feldpausch, T. R., Gloor, E., Baker, T. R., Lloyd, J., Lopez-Gonzalez, G., Monteagudo-Mendoza, A., Malhi, Y.,

& Lewis, S. L. (2015). Long-term decline of the Amazon carbon sink. *Nature*, *519*(7543), 344–348.

Brodribb, T. J., Powers, J., Cochard, H., & Choat, B. (2020). Hanging by a thread? Forests and drought. *Science*, *368*(6488), 261–266.

Cernusak, L. A., Winter, K., Dalling, J. W., Holtum, J. A., Jaramillo, C., Körner, C., Leakey, A. D., Norby, R. J., Poulter, B., & Turner, B. L. (2013). Tropical forest responses to increasing atmospheric CO_2: Current knowledge and opportunities for future research. *Functional Plant Biology*, *40*(6), 531–551.

Cox, P. M., Betts, R., Collins, M., Harris, P. P., Huntingford, C., & Jones, C. (2004). Amazonian forest dieback under climate-carbon cycle projections for the 21st century. *Theoretical and Applied Climatology*, *78*(1), 137–156.

de Almeida Castanho, A. D., Galbraith, D., Zhang, K., Coe, M. T., Costa, M. H., & Moorcroft, P. (2016). Changing Amazon biomass and the role of atmospheric CO_2 concentration, climate, and land use. *Global Biogeochemical Cycles*, *30*(1), 18–39.

De Guzman, M. E., Acosta-Rangel, A., Winter, K., Meinzer, F. C., Bonal, D., & Santiago, L. S. (2021). Hydraulic traits of neotropical canopy liana and tree species across a broad range of wood density: Implications for predicting drought mortality with models. *Tree Physiology*, *41*(1), 24–34.

Doughty, C. E., Metcalfe, D., Girardin, C., Amezquita, F. F., Cabrera, D. G., Huasco, W. H., Silva-Espejo, J., Araujo-Murakami, A., Da Costa, M., & Rocha, W. (2015). Drought impact on forest carbon dynamics and fluxes in Amazonia. *Nature*, *519*(7541), 78–82.

Eller, C. B., Rowland, L., Mencuccini, M., Rosas, T., Williams, K., Harper, A., Medlyn, B. E., Wagner, Y., Klein, T., & Teodoro, G. S. (2020). Stomatal optimization based on xylem hydraulics (SOX) improves land surface model simulation of vegetation responses to climate. *New Phytologist*, *226*(6), 1622–1637.

Esquivel-Muelbert, A., Galbraith, D., Dexter, K. G., Baker, T. R., Lewis, S. L., Meir, P., Rowland, L., da Costa, A. C. L., Nepstad, D., & Phillips, O. L. (2017). Biogeographic distributions of neotropical trees reflect their directly measured drought tolerances. *Scientific Reports*, *7*, 8334. https://doi.org/10.1038/s41598-017-08105-8

Esquivel-Muelbert, A., Phillips, O. L., Brienen, R. J., Fauset, S., Sullivan, M. J., Baker, T. R., Chao, K.-J., Feldpausch, T. R., Gloor, E., & Higuchi, N. (2020). Tree mode of death and mortality risk factors across Amazon forests. *Nature Communications*, *11*, 5515. https://doi.org/10.1038/s41467-020-18996-3

Feldpausch, T. R., Banin, L., Phillips, O. L., Baker, T. R., Lewis, S. L., Quesada, C. A., Affum-Baffoe, K., Arets, E. J. M. M., Berry, N. J., Bird, M., Brondizio, E. S., de Camargo, P., Chave, J., Djagbletey, G., Domingues, T. F., Drescher, M., Fearnside, P. M., França, M. B., Fyllas, N. M., … Lloyd, J. (2011). Height-diameter allometry of tropical forest trees. *Biogeosciences*, *8*(5), 1081–1106.

Feldpausch, T., Phillips, O., Brienen, R., Gloor, E., Lloyd, J., Lopez-Gonzalez, G., Monteagudo-Mendoza, A., Malhi, Y., Alarcón, A., & Dávila, E. Á. (2016). Amazon forest response to repeated droughts. *Global Biogeochemical Cycles*, *30*(7), 964–982.

Feng, X., Porporato, A., & Rodriguez-Iturbe, I. (2013). Changes in rainfall seasonality in the tropics. *Nature Climate Change*, *3*(9), 811–815.

Fisher, R., Williams, M., Da Costa, A. L., Malhi, Y., Da Costa, R., Almeida, S., & Meir, P. (2007). The response of an eastern Amazonian rain forest to drought stress: Results and modelling analyses from a throughfall exclusion experiment. *Global Change Biology*, *13*(11), 2361–2378.

Fleischer, K., Rammig, A., De Kauwe, M. G., Walker, A. P., Domingues, T. F., Fuchslueger, L., Garcia, S., Goll, D. S., Grandis, A., & Jiang, M. (2019). Amazon forest response to CO_2 fertilization dependent on plant phosphorus acquisition. *Nature Geoscience*, *12*(9), 736–741.

Franklin, J. F., Shugart, H. H., & Harmon, M. E. (1987). Tree death as an ecological process. *Bioscience*, *37*(8), 550–556.

Green, J. K., Berry, J., Ciais, P., Zhang, Y., & Gentine, P. (2020). Amazon rainforest photosynthesis increases in response to atmospheric dryness. *Science Advances*, *6*(47), eabb7232. https://doi.org/10.1126/sciadv.abb7232

Harris, I. (2020). *CRU JRA v2. 1: A forcings dataset of gridded land surface blend of climatic research unit (CRU) and Japanese reanalysis (JRA) data, January 1901–December 2019*. University of East Anglia Climatic Research Unit, Centre for Environmental Data Analysis.

Harris, I., Jones, P. D., Osborn, T. J., & Lister, D. H. (2014). Updated high-resolution grids of monthly climatic observations–the CRU TS3. 10 dataset. *International Journal of Climatology*, *34*(3), 623–642.

Harris, I., Osborn, T. J., Jones, P., & Lister, D. (2020). Version 4 of the CRU TS monthly high-resolution gridded multivariate climate dataset. *Scientific Data*, *7*, 109. https://doi.org/10.1038/s41597-020-0453-3

Holm, J. A., Knox, R. G., Zhu, Q., Fisher, R. A., Koven, C. D., Nogueira Lima, A. J., Riley, W. J., Longo, M., Negrón-Juárez, R. I., & de Araujo, A. C. (2020). The Central Amazon biomass sink under current and future atmospheric CO_2: Predictions from big-leaf and demographic vegetation models. *Journal of Geophysical Research: Biogeosciences*, *125*(3), e2019JG005500. https://doi.org/10.1029/2019JG005500

Hubau, W., Lewis, S. L., Phillips, O. L., Affum-Baffoe, K., Beeckman, H., Cuní-Sanchez, A., Daniels, A. K., Ewango, C. E., Fauset, S., & Mukinzi, J. M. (2020). Asynchronous carbon sink saturation in African and Amazonian tropical forests. *Nature*, *579*(7797), 80–87.

Janssen, T. A., Hölttä, T., Fleischer, K., Naudts, K., & Dolman, H. (2020). Wood allocation trade-offs between fiber wall, fiber lumen, and axial parenchyma drive drought resistance in neotropical trees. *Plant, Cell and Environment*, *43*(4), 965–980.

Jimenez, J. C., Libonati, R., & Peres, L. F. (2018). Droughts over Amazonia in 2005, 2010, and 2015: A cloud cover perspective. *Frontiers in Earth Science*, *6*, 227. https://doi.org/10.3389/feart.2018.00227

Jimenez, J. C., & Takahashi, K. (2019). Tropical climate variability and change: Impacts in the Amazon. *Frontiers in Earth Science*, *7*, 215. https://doi.org/10.3389/feart.2019.00215

Joetzjer, E., Maignan, F., Chave, J., Goll, D., Poulter, B., Barichivich, J., Maréchaux, I., Luyssaert, S., Guimberteau, M., & Naudts, K. (2022). Effect of tree demography and flexible root water uptake for modeling the carbon and water cycles of Amazonia. *Ecological Modelling*, *469*, 109969. https://doi.org/10.1016/j.ecolmodel.2022.109969

Kennedy, D., Swenson, S., Oleson, K. W., Lawrence, D. M., Fisher, R., Lola da Costa, A. C., & Gentine, P. (2019). Implementing plant hydraulics in the community land model, version 5. *Journal of Advances in Modeling Earth Systems*, *11*(2), 485–513.

Klein, T., Zeppel, M. J., Anderegg, W. R., Bloemen, J., De Kauwe, M. G., Hudson, P., Ruehr, N. K., Powell, T. L., von Arx, G., & Nardini, A. (2018). Xylem embolism refilling and resilience against drought-induced mortality in woody plants: Processes and trade-offs. *Ecological Research*, *33*(5), 839–855.

Kobayashi, S., Ota, Y., Harada, Y., Ebita, A., Moriya, M., Onoda, H., Onogi, K., Kamahori, H., Kobayashi, C., & Endo, H. (2015). The JRA-55 reanalysis: General specifications and basic characteristics. *Journal of the Meteorological Society of Japan. Series II*, *93*(1), 5–48.

Kunert, N., Zailaa, J., Herrmann, V., Muller-Landau, H. C., Wright, S. J., Pérez, R., McMahon, S. M., Condit, R. C., Hubbell, S. P., & Sack, L. (2021). Leaf turgor loss point shapes local and regional distributions of evergreen but not deciduous tropical trees. *New Phytologist*, *230*(2), 485–496.

Levine, N. M., Zhang, K., Longo, M., Baccini, A., Phillips, O. L., Lewis, S. L., Alvarez-Dávila, E., de Andrade, A. C. S., Brienen, R. J., & Erwin, T. L. (2016). Ecosystem heterogeneity determines the ecological resilience of the Amazon to climate change. *Proceedings of the National Academy of Sciences of the United States of America*, *113*(3), 793–797.

Lewis, S. L., Brando, P. M., Phillips, O. L., van der Heijden, G. M., & Nepstad, D. (2011). The 2010 Amazon drought. *Science*, *331*(6017), 554.

Li, L., Yang, Z. L., Matheny, A. M., Zheng, H., Swenson, S. C., Lawrence, D. M., Barlage, M., Yan, B., McDowell, N. G., & Leung, L. R. (2021).

Representation of plant hydraulics in the Noah-MP land surface model: Model development and multi-scale evaluation. *Journal of Advances in Modeling Earth Systems*, 13, e2020MS002214. https://doi.org/10.1029/2020MS002214

Liu, Y., Holtzman, N. M., & Konings, A. G. (2021). Global ecosystem-scale plant hydraulic traits retrieved using model–data fusion. *Hydrology and Earth System Sciences*, 25(5), 2399–2417.

Lu, Y., Duursma, R. A., Farrior, C. E., Medlyn, B. E., & Feng, X. (2020). Optimal stomatal drought response shaped by competition for water and hydraulic risk can explain plant trait covariation. *New Phytologist*, 225(3), 1206–1217.

Marthews, T. R., Quesada, C. A., Galbraith, D. R., Malhi, Y., Mullins, C. E., Hodnett, M. G., & Dharssi, I. (2014). High-resolution hydraulic parameter maps for surface soils in tropical South America. *Geoscientific Model Development*, 7(3), 711–723.

McCulloh, K. A., Domec, J. C., Johnson, D. M., Smith, D. D., & Meinzer, F. C. (2019). A dynamic yet vulnerable pipeline: Integration and co-ordination of hydraulic traits across whole plants. *Plant, Cell and Environment*, 42(10), 2789–2807.

Meakem, V., Tepley, A. J., Gonzalez-Akre, E. B., Herrmann, V., Muller-Landau, H. C., Wright, S. J., Hubbell, S. P., Condit, R., & Anderson-Teixeira, K. J. (2018). Role of tree size in moist tropical forest carbon cycling and water deficit responses. *New Phytologist*, 219(3), 947–958.

Mengis, N., Keller, D. P., Eby, M., & Oschlies, A. (2015). Uncertainty in the response of transpiration to CO_2 and implications for climate change. *Environmental Research Letters*, 10(9), 094001. https://doi.org/10.1088/1748-9326/10/9/094001

Mitchard, E. T., Feldpausch, T. R., Brienen, R. J., Lopez-Gonzalez, G., Monteagudo, A., Baker, T. R., Lewis, S. L., Lloyd, J., Quesada, C. A., & Gloor, M. (2014). Markedly divergent estimates of a mazon forest carbon density from ground plots and satellites. *Global Ecology and Biogeography*, 23(8), 935–946.

Naudts, K., Ryder, J., McGrath, M., Otto, J., Chen, Y., Valade, A., Bellasen, V., Berhongaray, G., Bönisch, G., & Campioli, M. (2015). A vertically discretised canopy description for ORCHIDEE (SVN r2290) and the modifications to the energy, water and carbon fluxes. *Geoscientific Model Development*, 8, 2035–2065.

Negrón-Juárez, R. I., Holm, J. A., Marra, D. M., Rifai, S. W., Riley, W. J., Chambers, J. Q., Koven, C. D., Knox, R. G., McGroddy, M. E., & Di Vittorio, A. V. (2018). Vulnerability of Amazon forests to storm-driven tree mortality. *Environmental Research Letters*, 13(5), 054021. https://doi.org/10.1088/1748-9326/aabe9f

Oliveira, R. S., Costa, F. R., van Baalen, E., de Jonge, A., Bittencourt, P. R., Almanza, Y., Barros, F. V., Cordoba, E. C., Fagundes, M. V., & Garcia, S. (2019). Embolism resistance drives the distribution of Amazonian rainforest tree species along hydro-topographic gradients. *New Phytologist*, 221(3), 1457–1465.

Papastefanou, P., Zang, C., Pugh, T., Liu, D., Lapola, D., Fleischer, K., Grams, T., Hickler, T., & Rammig, A. (2021). *New plant hydraulic architecture reproduces impacts of droughts in the Amazon rainforest*. Copernicus Meetings.

Papastefanou, P., Zang, C. S., Angelov, Z., de Castro, A. A., Jimenez, J. C., De Rezende, L. F. C., Ruscica, R., Sakschewski, B., Sörensson, A., & Thonicke, K. (2022). Recent extreme drought events in the Amazon rainforest: Assessment of different precipitation and evapotranspiration datasets and drought indicators. *Biogeosciences*, 19, 3843–3861. https://doi.org/10.5194/bg-19-3843-2022

Phillips, O. L., Aragão, L. E., Lewis, S. L., Fisher, J. B., Lloyd, J., López-González, G., Malhi, Y., Monteagudo, A., Peacock, J., & Quesada, C. A. (2009). Drought sensitivity of the Amazon rainforest. *Science*, 323(5919), 1344–1347.

Piao, S., Friedlingstein, P., Ciais, P., de Noblet-Ducoudré, N., Labat, D., & Zaehle, S. (2007). Changes in climate and land use have a larger direct impact than rising CO_2 on global river runoff trends.

Proceedings of the National Academy of Sciences of the United States of America, 104(39), 15242–15247.

Powell, T. L., Wheeler, J. K., de Oliveira, A. A., da Costa, A. C. L., Saleska, S. R., Meir, P., & Moorcroft, P. R. (2017). Differences in xylem and leaf hydraulic traits explain differences in drought tolerance among mature Amazon rainforest trees. *Global Change Biology*, 23(10), 4280–4293.

Powers, J. S., Vargas, G. G., Brodribb, T. J., Schwartz, N. B., Pérez-Aviles, D., Smith-Martin, C. M., Becknell, J. M., Aureli, F., Blanco, R., & Calderón-Morales, E. (2020). A catastrophic tropical drought kills hydraulically vulnerable tree species. *Global Change Biology*, 26(5), 3122–3133.

Ritchie, P., Clarke, J., Cox, P., & Huntingford, C. (2021). Overshooting tipping point thresholds in a changing climate. *Nature*, 592, 517–523.

Rowland, L., da Costa, A. C. L., Galbraith, D. R., Oliveira, R., Binks, O. J., Oliveira, A., Pullen, A., Doughty, C., Metcalfe, D., & Vasconcelos, S. (2015). Death from drought in tropical forests is triggered by hydraulics not carbon starvation. *Nature*, 528(7580), 119–122.

Rowland, L., Martínez-Vilalta, J., & Mencuccini, M. (2021). Hard times for high expectations from hydraulics: Predicting drought-induced forest mortality at landscape scales remains a challenge. *New Phytologist*, 230, 1685–1687.

Santiago, L. S., De Guzman, M. E., Baraloto, C., Vogenberg, J. E., Brodie, M., Hérault, B., Fortunel, C., & Bonal, D. (2018). Coordination and trade-offs among hydraulic safety, efficiency and drought avoidance traits in Amazonian rainforest canopy tree species. *New Phytologist*, 218(3), 1015–1024.

Signori-Müller, C., Oliveira, R. S., de Vasconcellos, B. F., Tavares, J. V., Gilpin, M., Diniz, F. C., Zevallos, M. J. M., Yupayccana, C. A. S., Acosta, M., & Bacca, J. (2021). Non-structural carbohydrates mediate seasonal water stress across Amazon forests. *Nature Communications*, 12, 2310. https://doi.org/10.1038/s41467-021-22378-8

Trugman, A. T., Anderegg, L. D., Anderegg, W. R., Das, A. J., & Stephenson, N. L. (2021). Why is tree drought mortality so hard to predict? *Trends in Ecology & Evolution*, 36(6), 520–532.

Wieder, W., Boehnert, J., Bonan, G., & Langseth, M. (2014). *Regridded harmonized world soil database v1.2*. ORNL DAAC.

Yang, X., Post, W., Thornton, P., & Jain, A. (2014). *Global gridded soil phosphorus distribution maps at 0.5-degree resolution*. ORNL DAAC.

Yang, Y., Saatchi, S. S., Xu, L., Yu, Y., Choi, S., Phillips, N., Kennedy, R., Keller, M., Knyazikhin, Y., & Myneni, R. B. (2018). Post-drought decline of the Amazon carbon sink. *Nature Communications*, 9, 3172. https://doi.org/10.1038/s41467-018-05668-6

Yao, Y., Joetzjer, E., Ciais, P., Viovy, N., Cresto Aleina, F., Chave, J., Sack, L., Bartlett, M., Meir, P., Fisher, R., & Luyssaert, S. (2022). Forest fluxes and mortality response to drought: Model description (ORCHIDEE-CAN-NHA r7236) and evaluation at the Caxiuanã drought experiment. *Geoscientific Model Development*, 15, 7809–7833. https://doi.org/10.5194/gmd-15-7809-2022

Yue, C., Ciais, P., Cadule, P., Thonicke, K., Archibald, S., Poulter, B., Hao, W., Hantson, S., Mouillot, F., & Friedlingstein, P. (2014). Modelling the role of fires in the terrestrial carbon balance by incorporating SPITFIRE into the global vegetation model ORCHIDEE–part 1: Simulating historical global burned area and fire regimes. *Geoscientific Model Development*, 7(6), 2747–2767.

Zemp, D. C., Schleussner, C.-F., Barbosa, H. M., Hirota, M., Montade, V., Sampaio, G., Staal, A., Wang-Erlandsson, L., & Rammig, A. (2017). Self-amplified Amazon forest loss due to vegetation-atmosphere feedbacks. *Nature Communications*, 8, 14681. https://doi.org/10.1038/ncomms14681

Zhang, K., de Almeida Castanho, A. D., Galbraith, D. R., Moghim, S., Levine, N. M., Bras, R. L., Coe, M. T., Costa, M. H., Malhi, Y., & Longo, M. (2015). The fate of Amazonian ecosystems over the coming century arising from changes in climate, atmospheric CO_2, and land use. *Global Change Biology*, 21(7), 2569–2587.

Ziegler, C., Coste, S., Stahl, C., Delzon, S., Levionnois, S., Cazal, J., Cochard, H., Esquivel-Muelbert, A., Goret, J.-Y., & Heuret, P. (2019). Large hydraulic safety margins protect neotropical canopy rainforest tree species against hydraulic failure during drought. *Annals of Forest Science*, *76*, 115. https://doi.org/10.1007/s13595-019-0905-0

Zuidema, P. A., Heinrich, I., Rahman, M., Vlam, M., Zwartsenberg, S. A., & van der Sleen, P. (2020). Recent CO_2 rise has modified the sensitivity of tropical tree growth to rainfall and temperature. *Global Change Biology*, *26*(7), 4028–4041.

Zuleta, D., Duque, A., Cardenas, D., Muller-Landau, H. C., & Davies, S. J. (2017). Drought-induced mortality patterns and rapid biomass recovery in a terra firme forest in the Colombian Amazon. *Ecology*, *98*(10), 2538–2546.

SUPPORTING INFORMATION

Additional supporting information can be found online in the Supporting Information section at the end of this article.